Experimental study of the microscopic mechanisms of magnetization reversal in FeNi/FeMn exchange-biased ferromagnet/antiferromagnet polycrystalline bilayers using the magneto-optical indicator film technique

V. S. Gornakov, Yu. P. Kabanov, O. A. Tikhomirov, and V. I. Nikitenko
Institute of Solid State Physics, Chernogolovka, 142432 Moscow Dhistrict, Russia

S. V. Urazhdin, F. Y. Yang, and C. L. Chien
The John Hopkins University, Baltimore, Maryland 21218, USA

A. J. Shapiro and R. D. Shull
National Institute of Standards and Technology, Gaithersburg, Maryland 20899, USA

(Received 31 January 2006; published 22 May 2006)

Remagnetization of the FeNi/FeMn bilayer was investigated using the magneto-optical indicator film imaging technique. We show the formation and breakdown of the homogeneous exchange spring into exchange springs of opposite chiralities during reversal in a rotating magnetic field. In reversal with a linear field, contrary to theoretical predictions, the winding of the exchange spring occurs without net magnetization rotation. It initiates by the formation of local spin spirals with opposite chirality and terminates with the formation of a single chiral state through the propagation of a specific kind of boundary separating regions with this single chirality from those with the mixed chiral state.

DOI: 10.1103/PhysRevB.73.184428 PACS number(s): 75.60.Ch, 75.60.Jk, 75.70.−i

I. INTRODUCTION

Exchange interaction at the interface of a ferromagnet (FM) and an antiferromagnet (AF) leads to a symmetry breaking of the magnetic constituent elements. The FM in the bilayer is characterized by a unidirectional anisotropy wherein opposite spin directions are energetically nonequivalent. The resultant striking exchange-bias phenomena,[1–4] with important practical applications,[5] have captured much attention in recent years. It is now recognized that the remagnetization of exchange-biased layers is determined by the uncompensated AF spins at the interface as well as by the nucleation and evolution of an exchange spring (or partial domain wall) parallel to the interface.[6–19] However, despite extensive research including experimental evidence of exchange spring, a coherent understanding of this phenomenon is still lacking.[20–27] One reason is that in real bilayers, both intralayer and interface imperfections can induce the formation of multidimensional exchange springs similar to the two-dimensional domain walls in bulk ferromagnets[28,29] or those in hard and soft ferromagnetic exchange-coupled bilayers.[30–37] In this work, we reveal the role of exchange springs of opposite chiralities in the remagnetization of exchange-coupled FM/AF bilayers.

II. EXPERIMENTAL DETAILS

The microscopic studies of the kinetics of the FM magnetization **M** in a FM/AF bilayer was provided by the magneto-optical indicator film (MOIF) technique,[32,38,39] which utilizes the high Faraday rotation and the in-plane anisotropy of a Bi-substituted iron garnet indicator film placed directly on top of the sample. The angle ψ of the polarization rotation of the garnet indicator film is proportional to the normal component $H_{\perp}^{MS}$ of the magnetostatic field produced by the underlying sample. Spatial maps of the magneto-optical signal are obtained with a polarizing microscope in the reflection mode using slightly uncrossed polarizers at a small angle β. In contrast to most previous studies of exchange bias, we used also a rotating magnetic field, well suited to reveal the exchange springs. To best reveal the rotation of **M**, we fabricated a 100 μm diameter hole in the sample and performed MOIF measurements around its edge. The magnetic poles on opposite sides of the hole permit a determination of both the orientation and magnitude of the average magnetization **M** of the surrounding region. The black and white colors of the magneto-optical image [Fig. 1(a)] correspond to opposite signs of $H_{\perp}^{MS}$. The magnitude of the perpendicular magnetostatic field is given by the intensity of the magneto-optical signal. For an in-plane **M** that is quasiuniform in the vicinity of the hole, the magneto-optical contrast is at a maximum along the symmetry axis of its magneto-optical stray field image. This axis is parallel to *M* and delineated by profile lines shown in Fig. 1(a). Photometric measurements of the magneto-optical signal intensity along this axis are shown in Fig. 1(b). Here the deviations from the mean intensity level (the gray background) of the

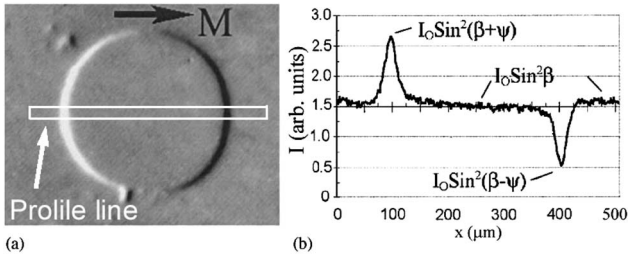

FIG. 1. (a) Magneto-optical image of a region of the sample containing a hole and (b) intensity of the magneto-optical signal along the profile line in (a).

 ©2006 The American Physical Society

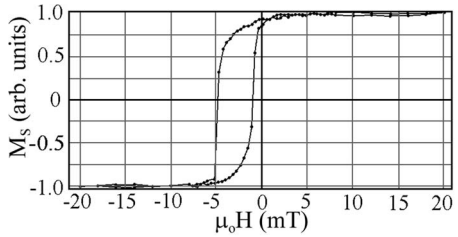

FIG. 2. Hysteresis loop of a NiFe/FeMn bilayer with H along the magnetic exchange anisotropy axis.

magneto-optical signal at the left and right side edges of the hole are, respectively, $I_L = I_O[\sin^2(\beta+\psi) - \sin^2\beta]$ and $I_R = I_O[\sin^2\beta - \sin^2(\beta-\psi)]$; where I_O is the intensity of the incident linearly polarized light. For small ψ, the average intensity $I_A = (I_L + I_R)/2 \sim \psi \sim H_\perp^{MS} \sim M$. Thus, the angular intensity profile caused by the leakage field from the hole edge gives the direction of **M**, while the intensity itself reflects the relative value of **M** averaged over the sample thickness.[32] The experimental results, including the chirality, are specific to the locations (FM or AF near the interface) at which the measurements were made.

For our study we used $Fe_{50}Mn_{50}$(30 nm)/$Ni_{81}Fe_{19}$(16 nm) bilayers that were sputter-deposited from alloy targets onto oxidized Si substrates at room temperature. A 30 nm thick Cu buffer layer was used to promote the growth of the antiferromagnetic fcc FeMn and ferromagnetic fcc $Ni_{81}Fe_{19}$ (permalloy=Py). A magnetic field of $\mu_0 H \approx 20$ mT was applied in the film plane during the deposition. After deposition, the samples were exchange-biased by heating to 440 K, followed by subsequent cooling to room temperature at $\mu_0 H = 1$ T along the deposition field direction.

III. RESULTS AND DISCUSSION

Figure 2 shows the hysteresis loop measured by a vibrating sample magnetometer with H directed along the magnetic anisotropy axis. This loop is typical of an exchange-biased FM with a bias field of $\mu_0 H_b = 3$ mT and a coercive force of $\mu_0 H_c = 1.9$ mT. We studied the exchange-spring formation by using a rotating **H** applied in the film plane and observed the region near the hole by the MOIF microscopy.

Figure 3 shows the dependences of the magneto-optical intensity $I_A(\varphi)$ and the angle $\alpha(\varphi)$ during counterclockwise (CCW) rotation of **H** at $\mu_o H = 2.4$ mT [Fig. 3(a)] and at a higher field of $\mu_o H = 3.0$ mT [Fig. 3(b)], over a range of φ, which is the angle between the field direction and the exchange anisotropy direction. The angle between **M** and the anisotropy axis is defined as α. In the initial state with a field rotation up to $\varphi \approx 100^\circ$, the magneto-optical signal remains practically unchanged. The behavior of $\alpha(\varphi)$ shows **M** rotation in the same direction as that of the field. However, **M** does not rotate in synchronization with the field, but lags behind. These results show that in these cases almost all of the FM spins rotate simultaneously and quasiuniformly. The significant lag angle of **M** is naturally explained by the spin spring formation in the AF layer near the interface.

Unusual results are revealed when φ is varied from about 100° to 170°. The value of average intensity I_A at the hole

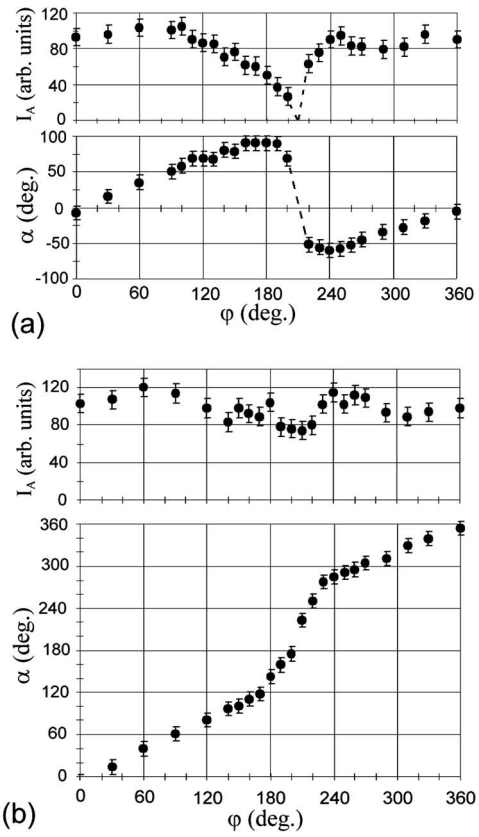

FIG. 3. Dependence of the average magneto-optical signal intensity I_A and the magnetization rotation angle α on the magnetic field rotation angle φ in the rotating field experiment at (a) $-\mu_0 H = 2.4$ mT and (b) $-\mu_0 H = 3.0$ mT.

edge decreases sharply, as shown in Fig. 3(a), but without any visible magneto-optical evidence (e.g., local black and white intensity modulation) of domain formation in the region surrounding the hole. In fact, I_A reaches practically zero at a critical angle of $\varphi_{cr} \approx 210^\circ$. In the case of a high field, as shown in Fig. 3(b), I_A reduces but does not vanish. These experimental results are in sharp contrast to theoretical estimations within the framework of the one-dimensional partial domain wall model. It is apparent that some spins in small domains (of nanoscale, which is below the spatial resolution of our technique) have changed their sense of rotation.

The presence of a complex exchange-spring structure, indicated by the unusual behavior shown in Fig. 3, is confirmed by MOIF images using a rotating field. Figures 4(a)–4(f) show the MOIF images for the CCW rotation of $\mu_0 H = 2.58$ mT over a range of φ. Figures 4(g)–4(l) show images for the same **H** value but for a clockwise (CW) rotation. The white arrow shows the direction of **H**, the black arrow and the compass needle in the hole show the direction of **M**, deduced from the MOIF contrast around the edge of the hole. We shall show below that the **H** value chosen for Fig. 4 is a critical value separating different rotation modes.

In the initial stages of rotation [Fig. 4(b)], there is little variation of **M**, and the MOIF signal at the hole edge is not significantly changed, indicating essentially a uniform **M** rotation both through the thickness and in the plane of the FM

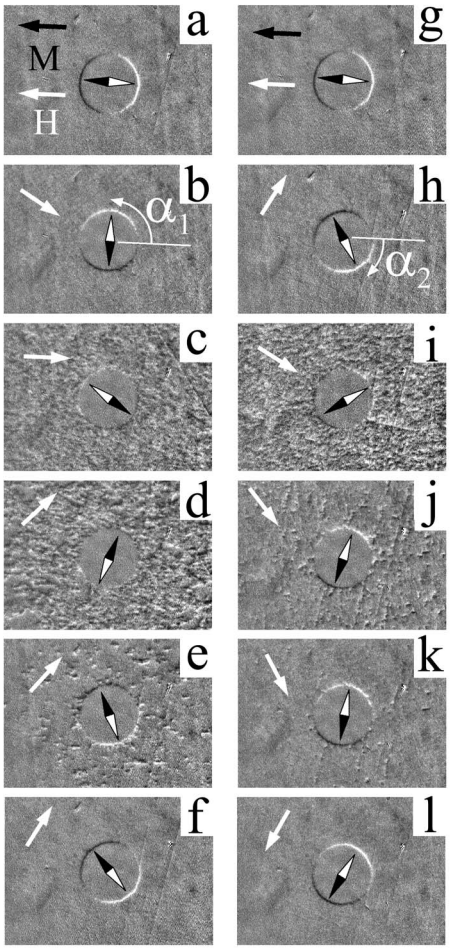

FIG. 4. MOIF images for H ($\mu_0 H$=2.58 mT) rotated to different angles from the exchange-bias direction: (a)–(f) are for H sequentially rotated counterclockwise to φ=0, 150°, 180°, 215°, 220°, 230°, and (g)–(l) are for H sequentially rotated clockwise to φ=0, −120°, −210°, −230°, −240°, and −300°, respectively.

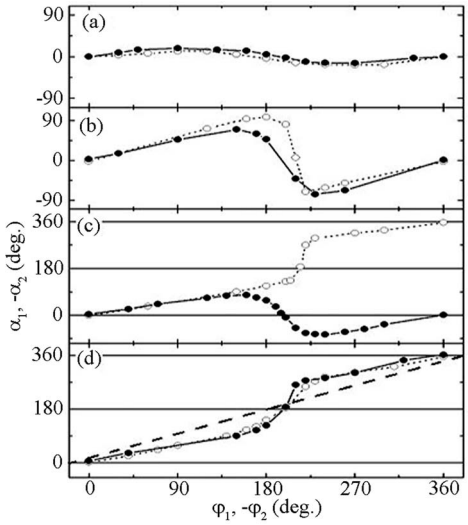

FIG. 5. Dependence of the magnetization orientation α on the field direction φ for counterclockwise (α_1, open symbols) and clockwise (α_2, filled symbols) field rotation from the exchange bias direction: Panels (a)–(d) are for $\mu_0 H$=0.6, 2.52, 2.58, and 3.0 mT, respectively. The dashed straight line in (d) shows the case for $\alpha = \varphi$.

layer. Subsequent to that several unusual features are revealed. When φ is near 180° [Figs. 4(c), 4(d), 4(i), and 4(j)], ripples in the MOIF images appear due to the significant local stray fields from the magnetic inhomogeneities. Simultaneously, the smaller intensity at the hole edge indicates a reduction of the net magnetization [Figs. 4(c) and 4(i)]. Note that for the CCW rotation, **M** initially follows the rotating **H** albeit with a lag [Figs. 4(a)–4(c)], whereas, in the later stages of rotation, **M** is actually *ahead* of the rotating field [Figs. 4(d)–4(f)]. However, the most striking features for CW **H** rotation are displayed in Figs. 4(i)–4(k). Initially, M rotates CW [Fig. 4(g) and 4(h)] but *reverses* to CCW rotation [Figs. 4(i)–4(k)] and with the appearance of magnetic ripples.

The above descriptions can be quantitatively displayed as α vs φ as shown in Fig. 5 for $\mu_0 H$=0.6, 2.52, 2.58, and 3 mT with the subscripts 1 and 2 referring to CCW and CW rotation, respectively. A small field (e.g., 0.6 mT) hardly perturbs **M**, and hence $\alpha \approx 0$ and independent of the sign of φ as shown in Fig. 5(a). At the other extreme [Fig. 5(d)], under a large field of 3 mT, **M** rotates in the same directions as **H** at all times, and hence α is always increasing ($\alpha = \varphi$ shown by the dashed straight line in Fig. 5(d), would be the limiting case of **M** strictly following **H**). The most unusual results, revealing the exchange spring, are those data shown for intermediate fields of 2.52 and 2.58 mT. At $\mu_0 H$=2.52 mT [Fig. 5(b)], α reaches its largest value of about 90° when $\varphi \approx 180°$ (i.e., when **H** is opposite to the exchange-bias axis), and α then returns to 0 while φ continues to increase past 180°. There is also a noticeable difference between the two opposite rotations. At the crossover field of H_{cr}=2.58 mT (the case shown in Fig. 5), the asymmetry between the opposite field rotation directions is most clearly revealed as shown in Fig. 5(c). We note that $|\alpha| \approx 90°$ appears to be the critical angle. For CCW rotation when M passes through $|\alpha| \approx 90°$, it continues to rotate to larger angles in a similar fashion to what is shown in Fig. 5(d) for higher field values. In contrast, for CW rotation [Fig. 5(c)], M may approach but never exceed $|\alpha| \approx 90°$ and varies with φ in a similar fashion to what is shown in Fig. 5(b) for a smaller field, even accompanied by a change of sign.

The unusual results in Figs. 4 and 5 reflect the formation of exchange springs and their evolution, indirectly revealed from the intensity experiment of Fig. 3. At small $|\varphi|$, the one-dimensional (uniform) exchange-spring chirality is determined by the rotation of the field. For intermediate field values, when $|\varphi| \approx 180°$ (Figs. 4 and 5), the dispersion in the direction of the exchange anisotropy axis leads to partial breakdown of the one-dimensional spring, and the formation of multiple local exchange springs with opposite chiralities (i.e., a multidimensional spring). Because of the spread in the local regions with an opposite orientation of M, the MOIF contrast around the hole edge also diminishes [Figs. 4, 5(c), 5(d), and 5(i)]. With further field rotation, the multidimensional exchange spring again becomes one-dimensional (i.e., with a single direction of winding), but with reversed chirality; for the largest φ values the magnitude of winding de-

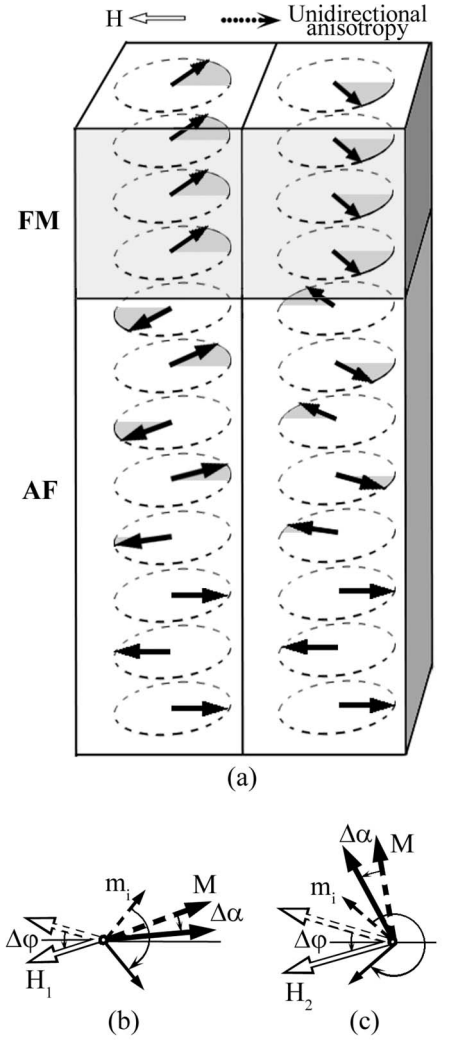

FIG. 6. (a) Schematic spin configuration near the interface during field reversal to a direction opposite the unidirectional anisotropy (K_A, dotted arrow). The effect of switching the local exchange-spring chirality on the net magnetization angle α under field rotation is shown in (b) and (c) under low field H_1 and high field H_2 conditions, respectively. Arrows in (b) and (c) show the orientations of H, M, and the local magnetization m_i before (dashed arrows) and after (solid arrows) m_i flop.

creases until it reaches zero at $|\varphi| = 360°$. The crossover between the "low field" and "high field" situations (Fig. 5) appears to be an abrupt response of the net magnetization when α reaches the critical value 90°. We will show that both regimes come from the same physical mechanism.

Due to a spatial dispersion of the unidirectional anisotropy axes in separate grains, the local exchange springs have different degrees of twisting, even in zero field, which can lead to an AF spin rotation with different twist directions [Fig. 6(a)]. When the field is applied and rotated sufficiently far ($\varphi \approx 180°$), the spring becomes unstable due to the high exchange energy of the extended exchange spring, and switching to the opposite chirality is preferable. The breakup of the exchange spring of the initial chirality occurs in separate grains, starting from those with the highest level of local

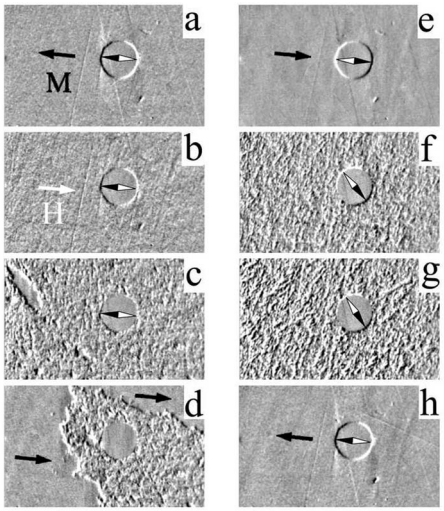

FIG. 7. MOIF images obtained during remagnetization with H directed along the exchange anisotropy axis: (a)–(d) are for decreasing $\mu_0 H = 0$, −3.6, −5.1, −5.28 mT, and (e)–(h) are for the subsequent increasing $\mu_0 H = -6$, −2.4, −0.3, and 3.0 mT, respectively.

spring twisting. The new direction of the local magnetization m_i after switching is approximately symmetrical about its own exchange anisotropy axis as shown in Fig. 6. However, the change of the net magnetization angle $\Delta\alpha$ resulting from any switching of the local exchange-spring chirality depends on the value of α. For low H and $\alpha < 90°$, the reflection of some spins about the exchange anisotropy axis causes $\Delta\alpha < 0$, i.e., an effective decrease of α [Fig. 6(b)]. For high H and $\alpha > 90°$, the partial switching of the exchange-spring chirality leads to an advance of the net magnetization with $\Delta\alpha > 0$ [Fig. 6(c)]. Precisely for this same reason, the effect of the local exchange-spring chirality on α is strong when the magnetic field is close to the critical field H_{cr}, and minimal when for $H \ll H_{cr}$ [Fig. 5(a)] or $H \gg H_{cr}$ [Fig. 5(d)].

Figures 4, 5(c), 5(d), and 5(i) demonstrate that the critical stage of the magnetization rotation, the breakdown of the original one-dimensional exchange-spring, proceeds through the formation of local exchange springs with opposite chiralities. We have found that the local exchange springs also play an important role in the usual magnetization reversal measurements, where a magnetic field of different values is applied along the exchange-bias direction as shown in Fig. 7. The magneto-optical images for the decreasing-field branch of the Fig. 2 hysteresis loop are shown in Figs. 7(a)–7(d). At $H = 0$ after saturation by a positive H [Fig. 7(a)], M is uniformly oriented along the exchange anisotropy axis. At $H < 0$, magnetic ripples appear, but M does *not* change its orientation, as deduced from the symmetry of the magneto-optical contrast around the hole. This observation is in variance with the predictions of simple exchange-spring models[6] assuming a monochiral rotational mode for magnetization reversal. Instead, local exchange springs with different degrees of twisting and opposite chiralities are formed. The topological barriers separating the exchange springs with opposite chiralities prevent them from coalescing to form a uniform reversed state. In this respect, the local exchange springs act as magnetization pinning centers. Figures

7(c) and 7(d) show that the overall reversal of M at larger negative H occurs through the gradual expansion of a new type of boundary separating the monochiral and polychiral regions. The formation and spread of this unusual phase boundary presents a new scenario for the magnetization reversal in exchange-bias systems, which to the best of our knowledge has not been described before.

Figures 7(e)–7(h) for the subsequent increasing-field branch present further evidence for the existence of a nonuniform spring with a single chirality in the reversed state. The reversal proceeds through a different mode than the decreasing-field branch. In particular, M first rotates to the direction presumably set by the chirality of the exchange spring. Figures 7(f) and 7(g) show that at $\mu_0 H \approx -2.4$ to -0.3 mT an intermediate inhomogeneous magnetization state is formed. In contrast to Figs. 7(c) and 7(d), the magnetic ripples disappear without a propagating front separating the inhomogeneous and a monodomain regions, because now the inhomogeneous state has local exchange springs with different degrees of twisting but with the same chiralities. The difference between the two reversal modes is due to the fact that unwinding of an already existing exchange-spring can proceed without any transformation of the exchange-spring structure as the process just corresponds to the release of stored energy. The accumulation of energy from the external field during a winding of the exchange spring in the decreasing-field branch inevitably faces resistance in the inhomogeneous medium and consequently may be accompanied by a local transformation of the spin structure like its chirality.

To date, some of developed models assume that the reversal of the ferromagnetic layer is uniform within its plane.[2,3,6–8,18] This view is prompted by the strong homogenizing exchange interactions within the ferromagnetic layer, and the high cost of the magnetostatic energy of the inhomogeneous state. A low intrinsic anisotropy of Py also favors a uniform rotation. This simplistic picture warrants major revisions in view of the drastically different reversal behavior with many incoherent characteristics evidenced in Figs. 4, 5, and 7. In particular, unlike the single crystal bilayer case,[10] where uniform macrodomains were formed during the magnetization reversal process, the dispersion of the exchange anisotropy axis in the polycrystalline bilayers provides different mechanisms of exchange-spring formation and interaction. The exchange interaction at the FM/AF interface varies locally in magnitude and direction, due to structural defects both in the interior and at the interfaces of the magnetic layers. In some theoretical models, such structural defects are responsible for the existence of the exchange bias itself.[3,11,20]

Our results demonstrate that during the magnetization reversal of the polycrystalline structure, the inhomogeneous exchange interaction at the interface can dominate the otherwise homogenizing effect of exchange interactions within the ferromagnetic layer. In the rotating field experiments, the driving torque can overcome the spatial dispersion of the exchange anisotropy axis to give an overall chirality of the exchange spring and to compel quasicontinuous magnetization rotation in high fields. In the linear field scanning experiments, there is no external factor breaking the chiral symmetry. The magnetization reversal in the decreasing-field branch of the hysteresis loop, corresponding to a tightening up of the exchange springs, proceeds through the propagation of a front separating the polychiral and monochiral regions. The reversal field value is not determined by the relative energies of the reversed and nonreversed magnetization orientations, as assumed by the simple exchange-bias models. Instead, pinning at the local inhomogeneities, which may well be the reason for the well-known but poorly understood enhancement of coercivity in exchange-biased ferromagnets, impedes the reversal. Finally, the magnetization reversal ends with the propagation of a new type of a front between a homogeneous state and an inhomogeneous state. Reversal back towards the exchange-bias direction proceeds through mostly homogeneous magnetization rotation, consistent with the expectations from the various exchange-spring models. In this case, local variations of exchange interaction still induce an inhomogeneous intermediate state (leading to an enhanced coercivity), but the topological barriers separating the exchange springs with opposite chiralities are absent. Consequently, the unwinding of the exchange spring occurs freely without the need for a new type of phase front.

IV. CONCLUSION

In conclusion, we have revealed the microscopic mechanisms of the formation and evolution of the exchange spring in exchange-biased systems. First, we demonstrated that the exchange spring exhibits an intrinsic chirality, which, at a certain critical field value, results in very different magnetization responses to a rotating magnetic field in opposite directions. Second, we demonstrated the crucial role played by the microscopically inhomogeneous states in the magnetization reversal process. We showed that the increasing- and decreasing-field reversals proceed through microscopically different mechanisms. The reversal against the exchange bias occurs through an inhomogeneous state of interacting microscopic exchange springs with opposite chiralities, followed by the propagation of a homogenizing front. We attribute this behavior to the existence of topological barriers separating the exchange springs with opposite chiralities. The reversal back toward the exchange-bias direction occurs through a mostly unichiral spin rotation, consistent with the one-dimensional exchange-spring models.

ACKNOWLEDGMENT

Work at JHU was supported by NSF Grant No. DMR04-03849.

[1] W. H. Meiklejohn and C. P. Bean, Phys. Rev. **102**, 1413 (1956); **105**, 904 (1957).
[2] J. Nogues and I. K. Schuller, J. Magn. Magn. Mater. **192**, 203 (1999).
[3] A. E. Berkowitz and K. Takano, J. Magn. Magn. Mater. **200**, 552 (1999).
[4] R. L. Stamps, J. Phys. D **33**, R247 (2000).
[5] B. Dieny, V. S. Speriosu, S. S. P. Parkin, B. A. Gurney, D. R. Wilhoit, and D. Mauri, Phys. Rev. B **43**, 1297 (1991).
[6] D. Mauri, H. C. Siegmann, P. S. Bagus, and E. Kay, J. Appl. Phys. **62**, 3047 (1987).
[7] N. C. Koon, Phys. Rev. Lett. **78**, 4865 (1997).
[8] T. C. Schulthess and W. H. Butler, Phys. Rev. Lett. **81**, 4516 (1998).
[9] N. J. Gokemeijer, T. Ambrose, and C. L. Chien, Phys. Rev. Lett. **79**, 4270 (1997).
[10] V. I. Nikitenko, V. S. Gornakov, L. M. Dedukh, Yu. P. Kabanov, A. F. Khapikov, A. J. Shapiro, R. D. Shull, A. Chaiken, and R. P. Michel, Phys. Rev. B **57**, R8111 (1998).
[11] M. D. Stiles and R. D. McMichael, Phys. Rev. B **59**, 3722 (1999).
[12] V. I. Nikitenko, V. S. Gornakov, A. J. Shapiro, R. D. Shull, Kai Liu, S. M. Zhou, and C. L. Chien, Phys. Rev. Lett. **84**, 765 (2000).
[13] I. N. Krivorotov, C. Leighton, J. Nogues, I. K. Schuller, and E. D. Dahlberg, Phys. Rev. B **68**, 054430 (2003).
[14] C. L. Chien, V. S. Gornakov, V. I. Nikitenko, A. J. Shapiro, and R. D. Shull, Phys. Rev. B **68**, 014418 (2003).
[15] M. R. Fitzsimmons, P. Yashar, C. Leighton, I. K. Schuller, J. Nogues, C. F. Majkrzak, and J. A. Dura, Phys. Rev. Lett. **84**, 3986 (2000).
[16] M. R. Fitzsimmons, C. Leighton, J. Nogues, A. Hoffmann, Kai Liu, C. F. Majkrzak, J. A. Dura, J. R. Groves, R. W. Springer, P. N. Arendt, V. Leiner, H. Lauter, and I. K. Schuller, Phys. Rev. B **65**, 134436 (2002).
[17] A. Scholl, M. Liberati, E. Arenholz, H. Ohldag, and J. Stohr, Phys. Rev. Lett. **92**, 247201 (2004).
[18] S. Roy, M. R. Fitzsimmons, S. Park, M. Dorn, O. Petracic, I. V. Roshchin, Zhi-Pan Li, X. Batlle, R. Morales, A. Misra, X. Zhang, K. Chesnel, J. B. Kortright, S. K. Sinha, and I. K. Schuller, Phys. Rev. Lett. **95**, 047201 (2005).
[19] J.-V. Kim and R. L. Stamps, Phys. Rev. B **71**, 094405 (2005).
[20] A. P. Malozemoff, Phys. Rev. B **35**, 3679 (1987).
[21] D. V. Dimitrov, S. Zhang, J. Q. Xiao, G. C. Hadjipanayis, and C. Prados, Phys. Rev. B **58**, 12090 (1998).
[22] K. Takano, R. H. Kodama, A. E. Berkowitz, W. Cao, and G. Thomas, Phys. Rev. Lett. **79**, 1130 (1997).
[23] H. Ohldag, T. J. Regan, J. Stohr, A. Scholl, F. Nolting, J. Luning, C. Stamm, S. Anders, and R. L. White, Phys. Rev. Lett. **87**, 247201 (2001).
[24] C. Leighton, M. R. Fitzsimmons, A. Hoffmann, J. Dura, C. F. Majkrzak, M. S. Lund, and I. K. Schuller, Phys. Rev. B **65**, 064403 (2002).
[25] B. Beckmann, U. Nowak, and K. D. Usadel, Phys. Rev. Lett. **91**, 187201 (2003).
[26] O. de Haas, R. Schafer, L. Schultz, K.-U. Barholz, and R. Mattheis, J. Magn. Magn. Mater. **260**, 380 (2003).
[27] P. Kappenberger, S. Martin, Y. Pellmont, H. J. Hug, J. B. Kortright, O. Hellwig, and Eric E. Fullerton, Phys. Rev. Lett. **91**, 267202 (2003).
[28] A. P. Malozemoff and J. C. Slonczewski, *Magnetic Domain Walls in Bubble Materials* (Academic, New York, 1979).
[29] A. Hubert and R. Shafer, *Magnetic Domains* (Springer, Berlin, 1998).
[30] R. D. Shull, A. J. Shapiro, V. S. Gornakov, V. I. Nikitenko, J. S. Jiang, H. Kaper, G. Leaf, and S. D. Bader, IEEE Trans. Magn. **37**, 2576 (2001).
[31] J. S. Jiang, S. D. Bader, H. Kaper, G. K. Leaf, R. D. Shull, A. J. Shapiro, V. S. Gornakov, V. I. Nikitenko, C. L. Platt, A. E. Berkowitz, S. David, and E. E. Fullerton, J. Phys. D **35**, 2339 (2002).
[32] V. S. Gornakov, V. I. Nikitenko, A. J. Shapiro, R. D. Shull, J. S. Jiang, and S. D. Bader, J. Magn. Magn. Mater. **246**, 80 (2002).
[33] V. I. Nikitenko, V. S. Gornakov, Yu. P. Kabanov, A. J. Shapiro, R. D. Shull, C. L. Chien, J. S. Jiang, and S. D. Bader, J. Magn. Magn. Mater. **258-259**, 19 (2003).
[34] V. S. Gornakov, Yu. P. Kabanov, V. I. Nikitenko, O. A. Tikhomirov, A. J. Shapiro, and R. D. Shull, JETP **99**, 602 (2004).
[35] F. Montaigne, S. Mangin, and Y. Henry, Phys. Rev. B **67**, 144412 (2003).
[36] Y. Henry, S. Mangin, and F. Montaigne, Phys. Rev. B **69**, 140401(R) (2004).
[37] S. Mangin, C. Bellouard, S. Andrieu, F. Montaigne, P. Ohresser, N. B. Brookes, and B. Barbara, Phys. Rev. B **70**, 014401 (2004).
[38] L. A. Dorosinskii, M. V. Indenbom, V. I. Nikitenko, Yu. A. Ossip'yan, A. A. Polyanskii, and V. K. Vlasko-Vlasov, Physica C **203**, 149 (1992).
[39] L. H. Bennett, R. D. McMichael, L. J. Swartzendruber, S. Hua, D. S. Lashmore, A. J. Shapiro, V. S. Gornakov, L. M. Dedukh, and V. I. Nikitenko, Appl. Phys. Lett. **66**, 888 (1995).